Figure Legends

Figure 1. MENβ is a potent RNA component for paraspeckle formation. A. MENβ, but not MENε, rescued paraspeckle formation. Intact paraspeckles were detected by RNA-FISH with the antisense probe of mouse MENε/β ncRNAs and coimmunostaining of endogenous PSF. Paraspeckles, which were observed in wild-type MEF cells (WT), were undetectable in MEF cells prepared from MENε/β-knockout mice (KO). Paraspeckles were detected in KO-MEF cells transfected with a plasmid expressing MENε (KO+MENε) or MENβ (KO+MENβ). **B.** Effect of actinomycin D treatment on the reformed paraspeckle-like foci. KO-MEF cells were cotransfected with plasmids expressing MENβ ncRNA and PSF-Flag. Transfected cells were treated with 0.3 μg/mL actinomycin D for 4 h. Reformed paraspeckle-like foci were visualized with RNA-FISH of MENε/β and coimmunostained with anti-Flag M2 antibody. **C.** MENβ ncRNA is more competent than MENε ncRNA at elevating the number of paraspeckles. NIH3T3 cells were cotransfected with expression plasmids of control (+control), MENε (+MENε), or MENβ (+MENβ), together with PSF-Flag. The counted paraspeckle numbers are shown in Figure S1C. Scale bar, 10 μm.

Figure 2. Identification of novel paraspeckle protein (PSP) components. A. Experimental strategy to identify new PSPs. **B.** Selection of FLJ-Venus clones that localize to paraspeckle-like nuclear foci. Paraspeckles were visualized by the immunostaining of PSF. Three representatives (PSP10, PSP14, and PSP33) of the new PSPs are shown. **C.** Confirmation of the paraspeckle localization of endogenous PSP counterparts. Antibodies against each

counterpart of PSP10, PSP14, and PSP33 (EWSR1, FUS and TAF15, respectively) were employed to monitor the localization (see Table S4). MENε/β ncRNAs were used as paraspeckle markers. **D**. Effect of actinomycin D treatment on the localization patterns of selected PSPs. Localization of the Venus clones in B was monitored after actinomycin D treatment. PSF is an endogenous PSP control. Data regarding other PSPs are shown in Figures S2 and S3. Scale bar, 10 μm.

Figure 3. Functional assignment of new PSPs in paraspeckle formation by extensive RNAi treatment. The paraspeckle appearance and MENε/β levels were monitored by RNA-FISH and RNase protection assay (RPA) to detect MENε and MENβ. **A**. Schema for the RPA probe used and the protected fragments (with size, nt) of MENε and MENβ. **B**. Paraspeckles in cells treated with control siRNA. Data for a representative from each category (1A: PSP2, 1B: PSP8/DAZAP1, 2: PSP21/hnRNP R, 3A: PSP34/UBAP2L, 3B: PSP36/ZNF335) are shown in **C**, **D**, **E**, **F**, and **G**, respectively. The siRNA numbers (#) used in the RNA-FISH analysis are shown at the lower left of each photo. For RPA, the ratio of band intensities of two isoforms, normalized by those of U12 snRNA, are shown below (Ctl was defined as 100%). RNAi data regarding all PSPs are compiled in Figure S5. Their quantified data are shown in Table S3. siRNAs used are shown in Table S6. Scale bar, 10 μm.

Figure 4. Alternative 3'-end processing of MENε/β is the initial essential step underlying paraspeckle formation. A. PSPs required for the alternative

3'-end processing of MENε/β. RPA was performed as in Figure 3. Data are shown for CFIm25 and CFIm68, which are required for MENε 3'-end processing, and hnRNP K, which is required for MENβ synthesis by interfering with MENε 3'-end processing. **B.** Paraspeckle appearance in HeLa cells treated with siRNAs against CFIm25, CFIm68, or hnRNP K. **C.** Plasmid rescue of a defect of MENβ synthesis in hnRNP K-eliminated cells. Two siRNAs against hnRNP K (K#2 and K#3) were used to eliminate endogenous hnRNP K, and hnRNP K rescue plasmid (K) was introduced at three concentrations (1–5 μg). MENε/β ncRNA levels were measured by RPA as in Figure 3. The ratios of MENε to MENβ are shown below the upper panel (MENε/MENβ). GADPH and hnRNP K were detected by Western blotting (WB). **D**. Paraspeckle formation rescued by expression of hnRNP K from the plasmid. The siRNAs and rescue plasmids used are shown on the left and the top, respectively. Paraspeckles were detected by RNA-FISH of MENε/β. Transfected cells were visualized by immunostaining with αFlag. Paraspeckles that formed in the rescued cells are shown by arrowheads. Scale bar, 10 μm. **E**. Quantification of the results in D. Cells possessing more than one paraspeckle-like focus were counted. siRNAs used are shown in Table S6. *P*-value was calculated by Student's *t*-test.

Figure 5. Roles of CFIm and hnRNP K in 3'-end processing of MENε. A. Schematics of substrate RNAs for the in vitro processing reaction that contains the region spanning the MENε 3'-end. Numbers indicate distance from the polyadenylation site of MENε. Middle scheme represents putative sequences around the MENε 3'-end processing site that are recognized by the CFIm

complex (CFBS: red boxes) and hnRNP K (KBS: blue box), respectively. The mutated positions on the mutant substrates (CFIm-mut, K-mut and PAS-mut) are shown. **B.** Recapitulation of CFIm-dependent 3'-end processing of MENε in vitro. Incubation time is shown above each panel. Substrate RNAs are represented on the top. Unprocessed and processed bands are shown by closed and open triangles, respectively, on the right. Processing efficiencies (%) are shown below each panel. **C**. Average values of the processing efficiencies obtained from three independent experiments are plotted on the graph. **D.** Detection of sequence-specific RNA-binding of hnRNP K. Gel mobility shift assay to detect binding of recombinant hnRNP K protein (r-K) with RNA fragments (30 nt) derived from WT and K-mut, WT oligo, and K-mut oligo, respectively, are shown. The RNA-protein complex and free RNA are shown by closed and open triangles, respectively. The amounts of r-K supplemented (μg) are shown above each panel.

Figure 6. Molecular mechanism of the alternative 3'-end processing of MENε/β. A. Detection of RNA-binding of CFIm during in vitro processing by UV-crosslinking. UV-crosslinked WT substrate RNA-binding proteins were detected as ^{32}P-labeled proteins on SDS-PAGE. The 68- and 25-kDa UV-crosslinked RNA-binding proteins (closed and open arrows, respectively) were immunoprecipitated with antibodies against CFIm68 and CFIm25. **B.** RNA-bindings of CFIm68 and CFIm25 are affected by the addition of r-K. The two RNA substrates (WT and K-mut) employed are shown on the top. Addition of r-K (+) at two concentrations (10x and 30x excess of endogenous hnRNP K in

HNE) and incubation time (min) are shown above. Closed and open triangles are as in A. The intensities of 68 and 25 kDa were quantified and normalized by the levels of CFIm68 and CFIm25, respectively, which were detected by the Western blot (WB) shown below. Molecular weight marker is shown on the left. **C**. Confirmation of r-K–dependent inhibition of RNA-binding of CFIm68 and CFIm25. Presence (+) or absence (-) of r-K (30x excess) is indicated above the panel. UV-crosslinking of r-K (~55 kDa) was detected in Input lane (+r-K) and in Figure S7B. Closed and open triangles are as in A. Amounts of CFIm25 in the input samples and immunoprecipitated samples were detected by the WB shown below the panel. **D**. Quantification of immunoprecipitated, UV-crosslinked CFIm25 in presence (+) or absence (-) of r-K (open triangle in the upper pane in C). Data were normalized with the total amounts of CFIm25 in each immunoprecipitation sample (lower panel in C). Graph shows average (with SD) of three independent experiments. *P*-value was calculated by Student's *t*-test. **E**. Quantification of immunoprecipitated CFIm68, as in D. **F**. Interaction between hnRNP K and CFIm25 in vivo. Immunoprecipitations with αCFIm25 and αCFIm68 were performed in the presence (+) or absence (-) of RNase A. CFIm68, CFIm25, and hnRNP K were detected by WB. **G**. CFIm68-CFIm25 interaction is affected by hnRNP K. HNE was incubated with r-K in the presence of WT RNA. Immunoprecipitation with αCFIm25 was performed in the presence (+) or absence (-) of r-K. CFIm68, CFIm25, hnRNP K, and GAPDH were detected by WB. Immunoprecipitation of CFIm68 was diminished in the presence of r-K. **H**. Quantification of immunoprecipitated CFIm68 in the presence or absence of r-K. Relative amount (%) of CFIm68 was normalized by

the immunoprecipitated CFIm25 level (**G**). Average values (n = 3) are plotted. *P*-value was calculated by Student's *t*-test. Asterisk represents nonspecific binding of excess r-K to IgG. Lane numbers are shown below (**A**, **B**, **F**, and **G**). Antibodies used are shown in Table S4. **I.** Models of MENε/β isoform synthesis. MENε/β border region is shown with the critical sequence elements. Pathways for MENε and MENβ synthesis are shown above and below the MENε/β scheme. For MENβ synthesis, hnRNP K binds with the UCCCCUU sequence, captures CFIm25 from the functional CFIm (CFIm68-CFIm25 heterodimer), and results in the arrest of CFIm-binding to upstream UGUA sequences.

Table 1

Table 1. Paraspeckle proteins

Proteins			Accession	RNA-binding Motifs	Other Motifs	Category
PSP #	HUGO	Synonyms				
New paraspeckle proteins						
PSP3	AHDC1		Q5TGY3		AT hook	3B
PSP4	AKAP8L		Q9ULX6		2 ZnF C2H2s	3B
PSP5	CELF6	BRUNOL6	Q96J87	3 RRMs		N.D.
PSP6	CIRBP		Q14011	RRM		3B
PSP7	CPSF7	CFIm59	Q8N684	RRM		2
PSP8	DAZAP1		Q96EP5	2 RRMs		1B
PSP9	DLX3		O60479		homeodomain	N.D.
PSP10	EWSR1		Q01844	RRM	ZnF RanBP2	3B
PSP11	FAM98A		Q8NCA5			2
PSP12	FAM113A		Q9H1Q7			2
PSP13	FIGN		Q5HY92			2
PSP14	FUS	TLS	P35637	RRM	ZnF RanBP2	1B
PSP15	HNRNPA1		P09651	2 RRMs		2
PSP16	HNRNPA1L2		Q32P51	2 RRMs		N.D.
PSP17	HNRNPF		P52597	3 RRMs		N.D.
PSP18	HNRNPH1		P31943	3 RRMs		N.D.
PSP19	HNRNPH3		P31942	2 RRMs		1B
PSP20	HNRNPK		P61978	3 KHs		1A
PSP21	HNRNPR		O43390	3 RRMs		2
PSP22	HNRNPUL1		Q9BUJ2		SAP, SPRY	2
PSP23	MEX3C		Q5U5Q3	2 KHs	ZnF RING	N.D.
PSP24	NUDT21	CFIm25	O43809		NUDIXhydrolase	3A
PSP25	RBM3		P98179	RRM		3B
PSP26	RBM4B	RBM30	Q9BQ04	2 RRMs	ZnF CCHC	3B
PSP27	RBM7		Q9Y580	RRM		3B
PSP28	RBM12		Q9NTZ6	3 RRMs		2
PSP29	RBMX		P38159	RRM		3B
PSP30	RUNX3		Q13761			3B
PSP31	SRSF10	FUSIP1, SRp38	O75494	RRM	RS	2
PSP32	SS18L1		O75177			N.D.
PSP33	TAF15		Q92804	RRM	ZnF RanBP2	2
PSP34	UBAP2L		Q14157			3A
PSP35	ZC3H6		P61129		3 ZnF C3H1s	3B
PSP36	ZNF335		Q9H4Z2		13ZnF C2H2s	3B
TDP43	TARDBP	ALS10	Q13148	2 RRMs		2
Known paraspeckle proteins						
CFIm68	CPSF6		Q16630	RRM		3A
p54nrb	NONO		Q15233	2 RRMs		1A
PSP1	PSPC1		Q8WXF1	2 RRMs		3B
PSP2	RBM14	CoAA	Q96PK6	2 RRMs		1A
PSF	SFPQ		P23246	2 RRMs		1A

Figure 1
Click here to download high resolution image

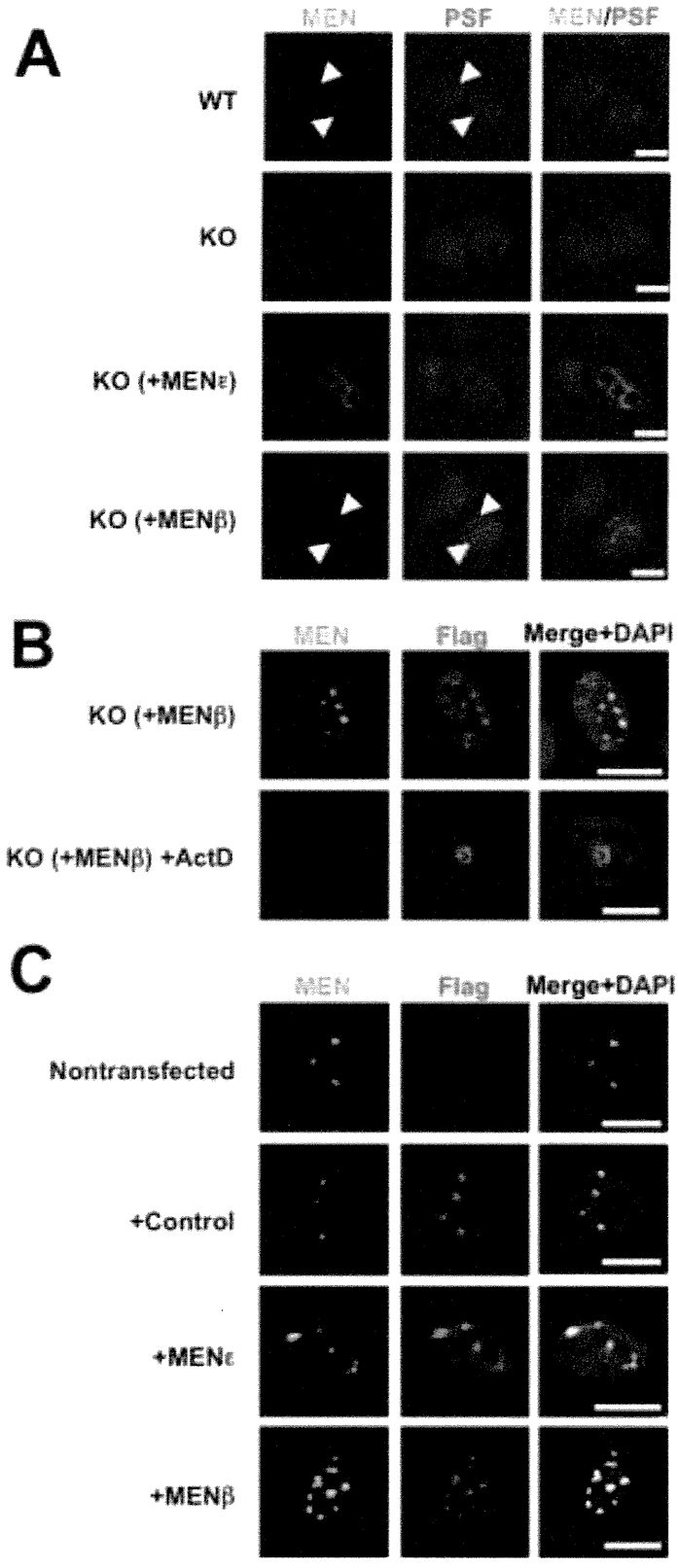

Figure 2
Click here to download high resolution image

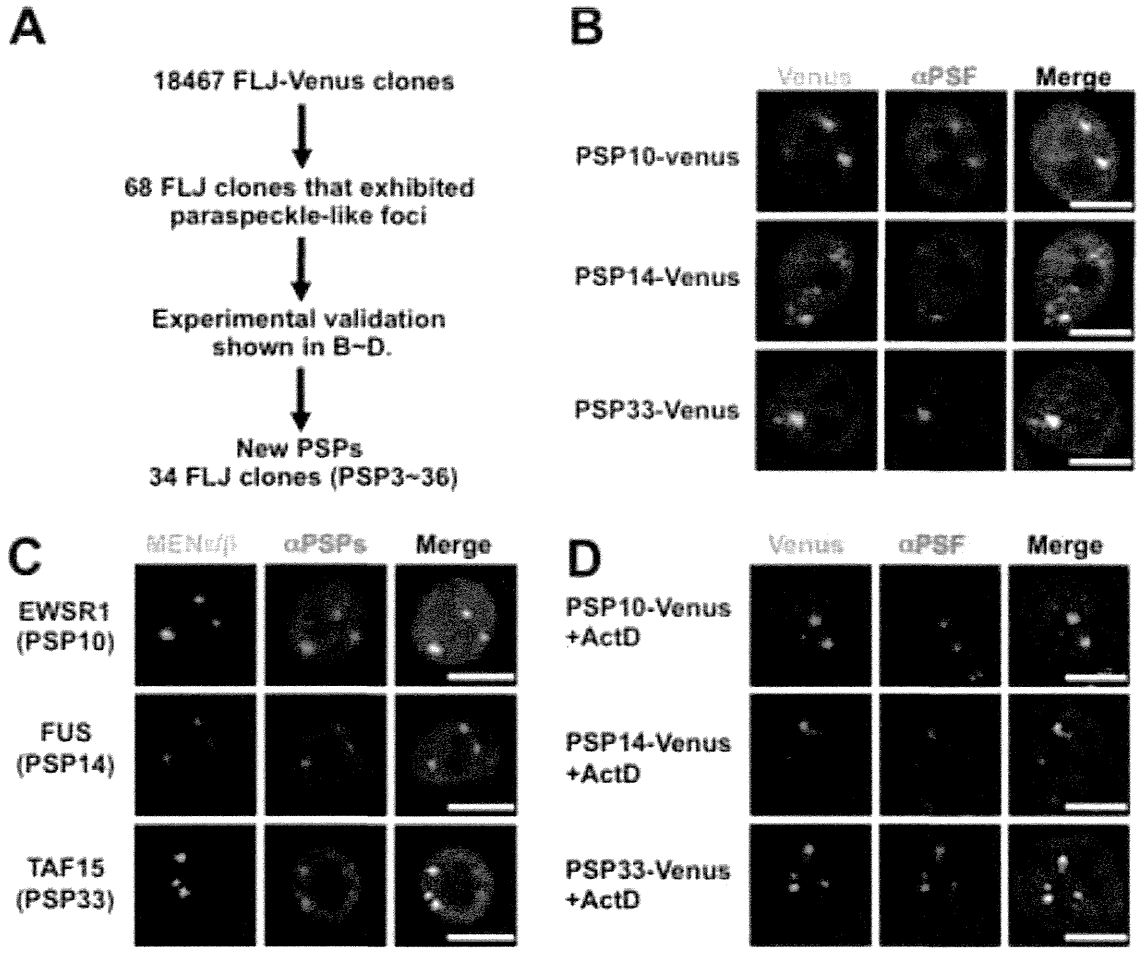

Figure 3
Click here to download high resolution image

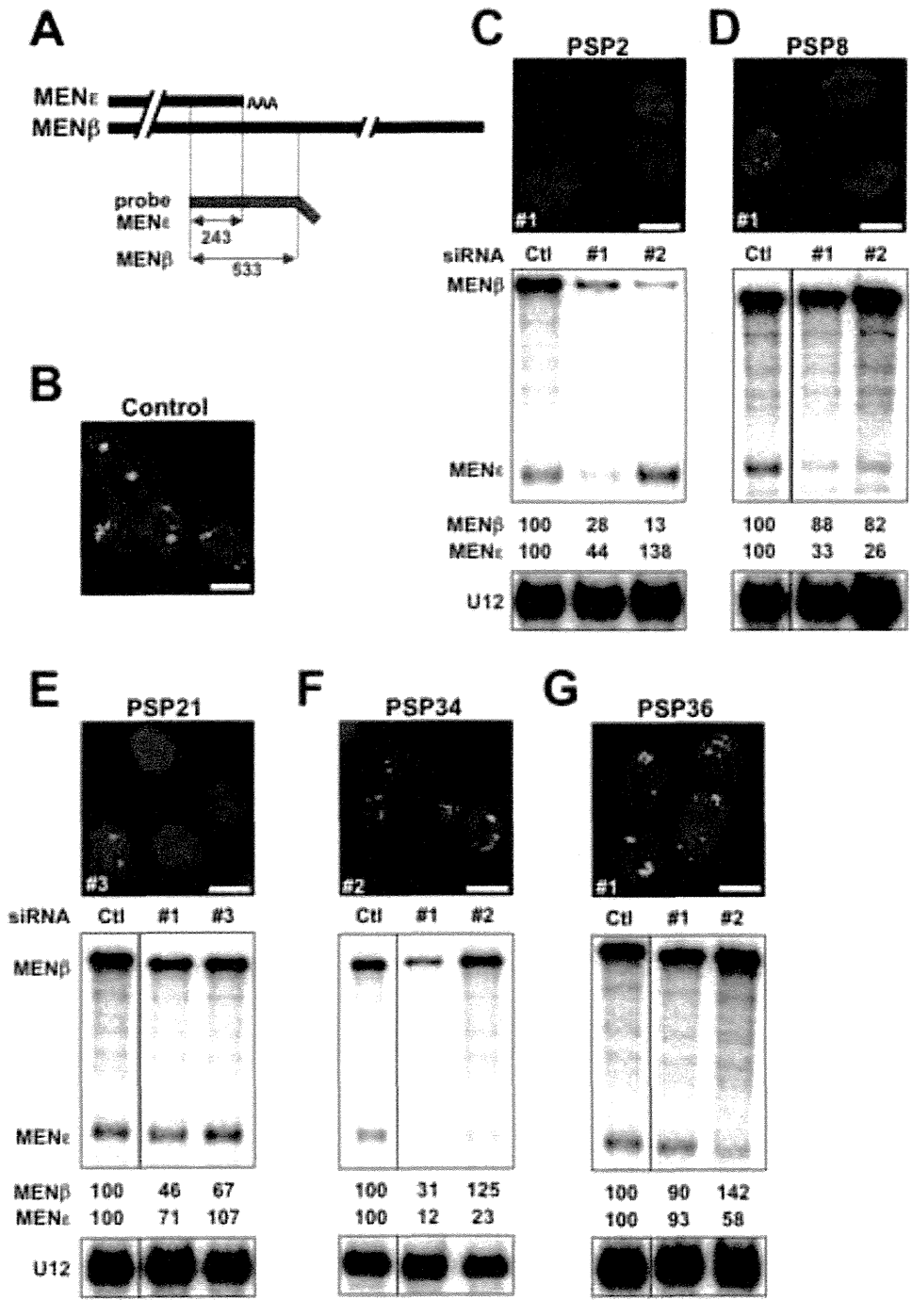

Figure 4
Click here to download high resolution image

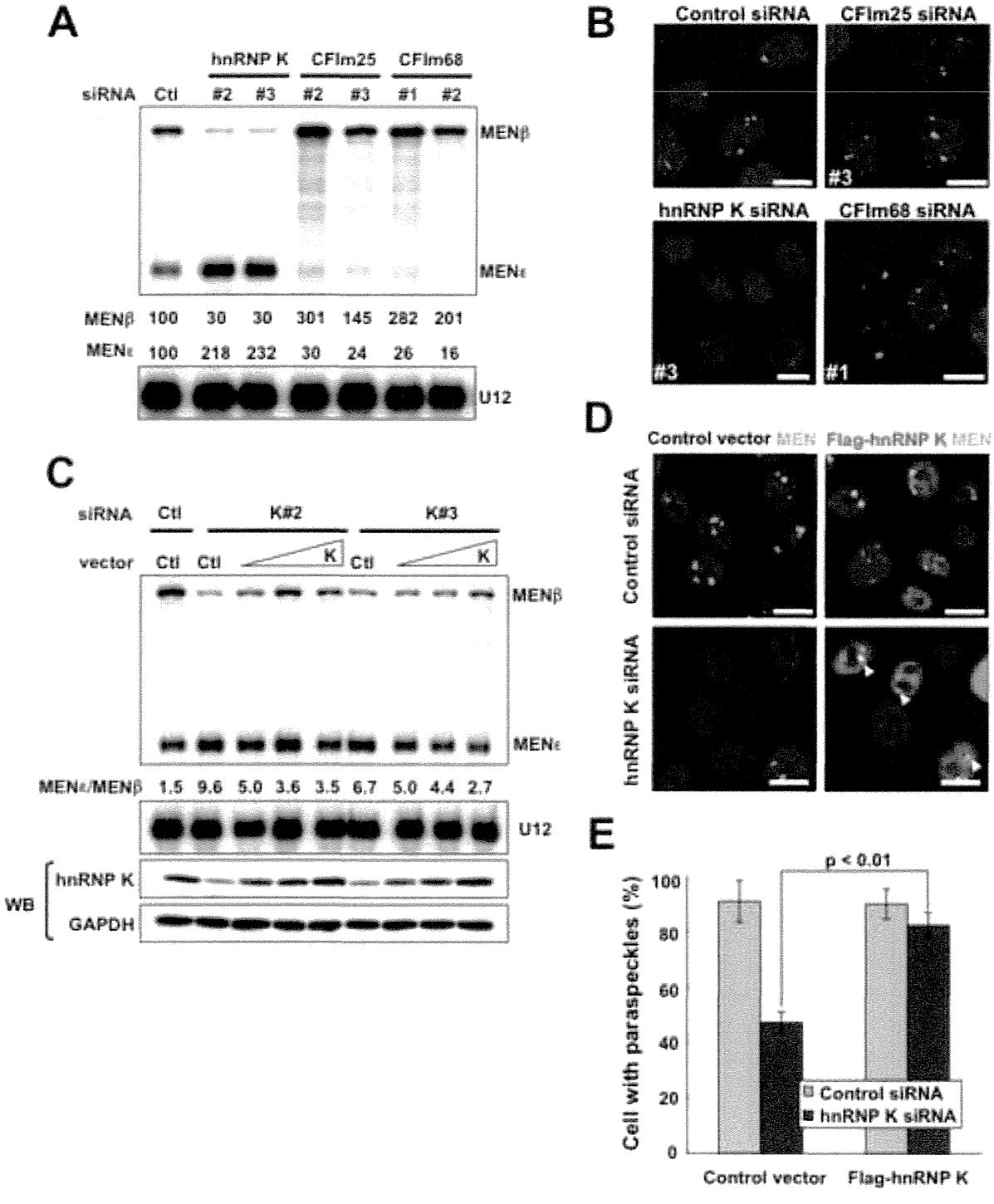

Figure 5
Click here to download high resolution image

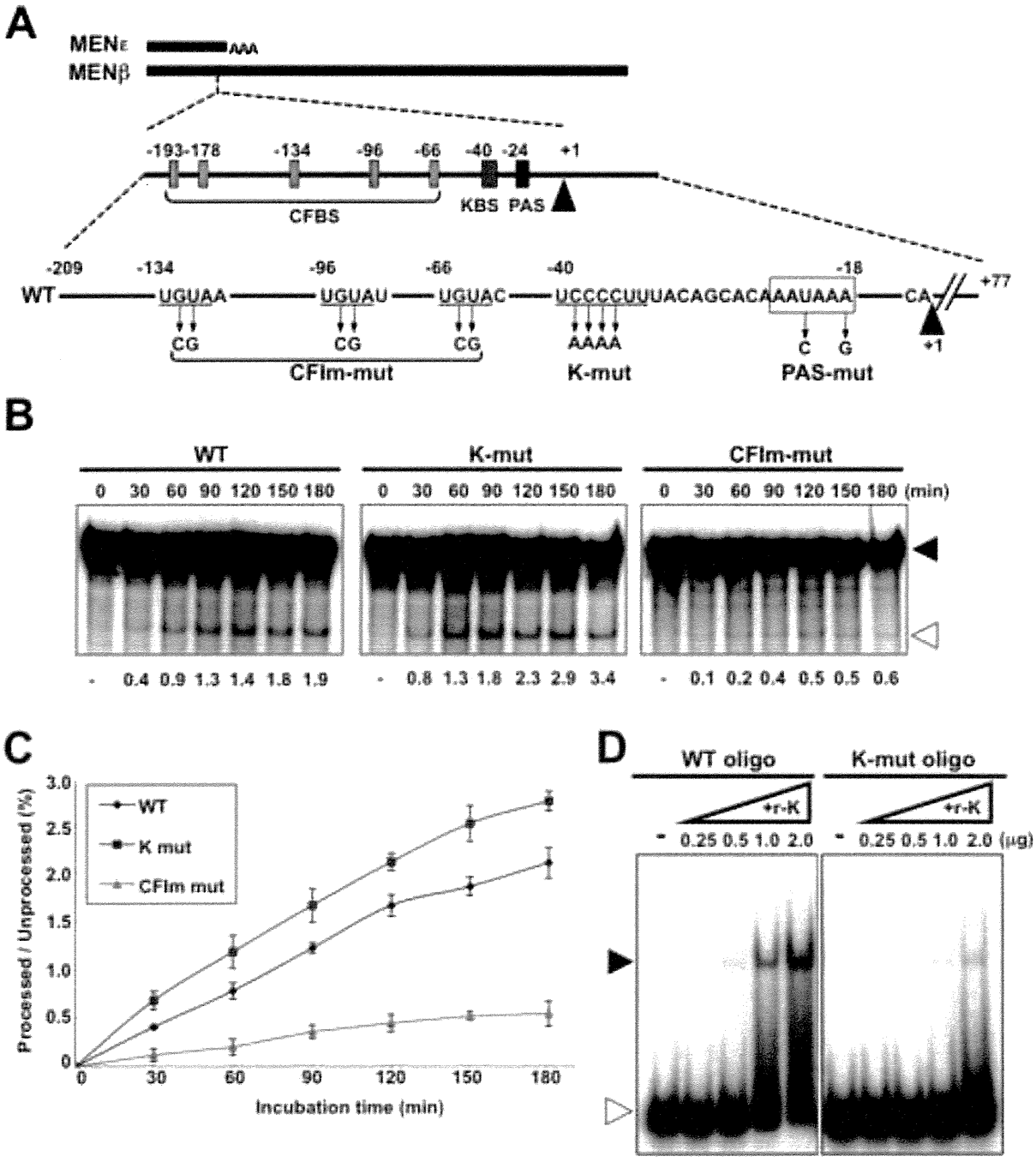

Figure 6
Click here to download high resolution image

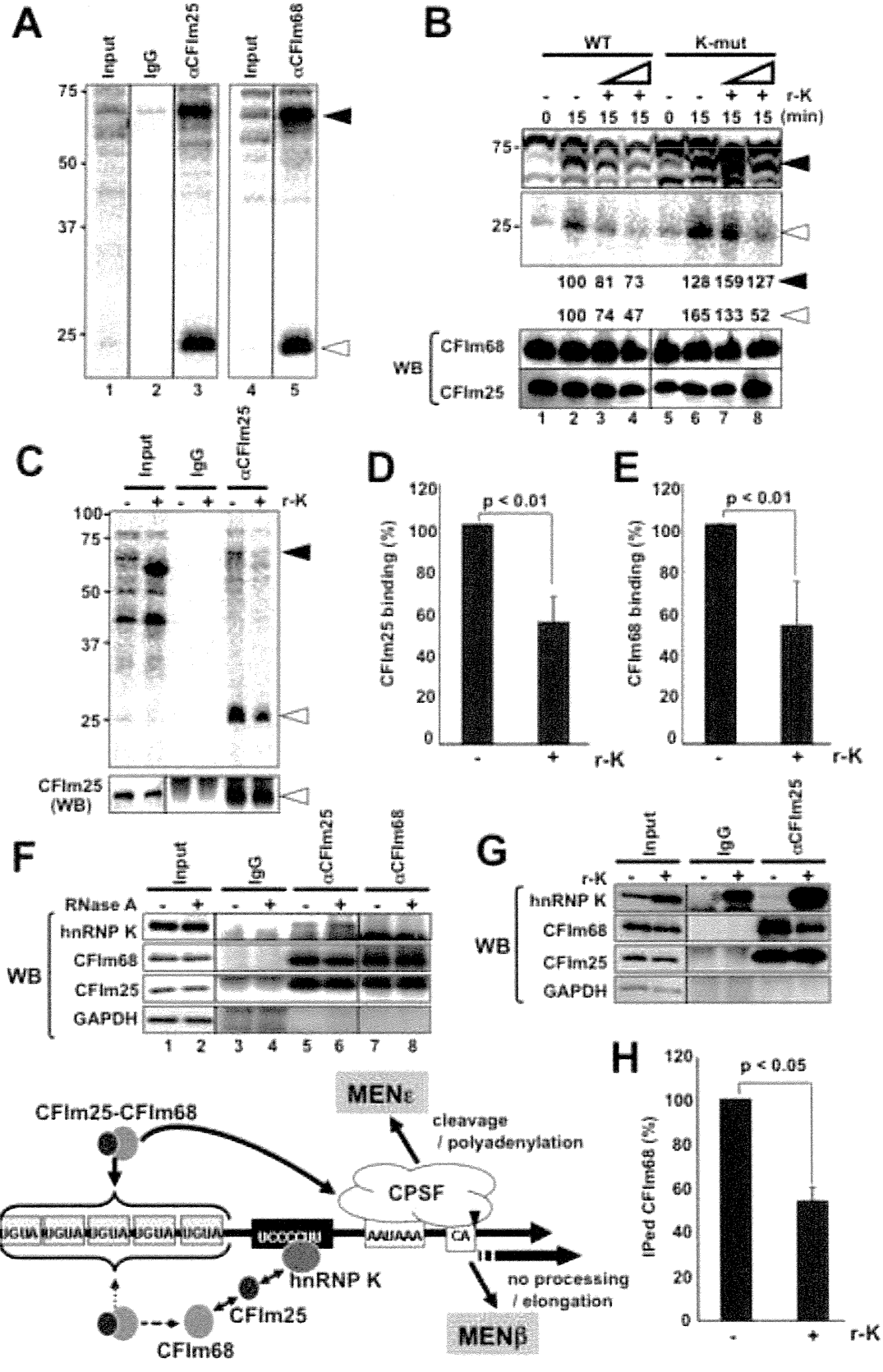

Inventory of Supplemental Information

Figure S1

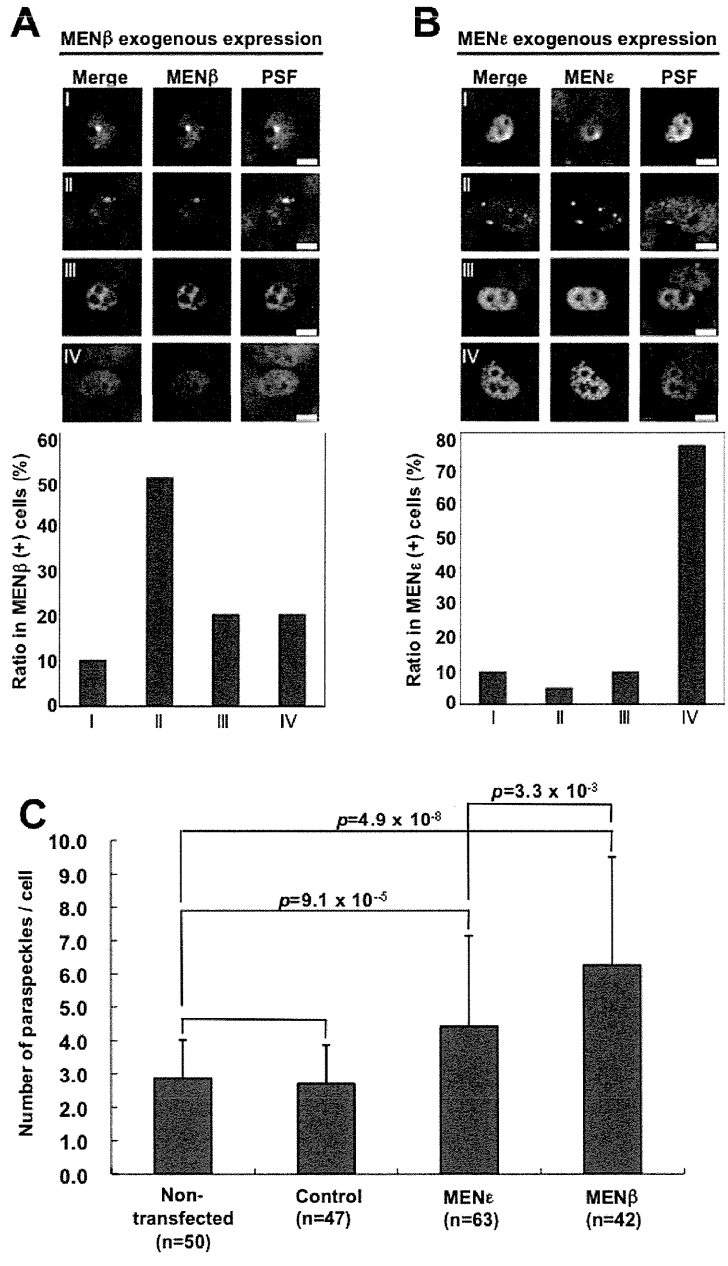
A
MENβ exogenous expression
Merge
MENβ
PSF
I
II
III
IV
Ratio in MENβ (+) cells (%)
60
50
40
30
20
10
0
I
II
III
IV
B
MENε exogenous expression
Merge
MENε
PSF
I
II
III
IV
Ratio in MENε (+) cells (%)
80
70
60
50
40
30
20
10
0
I
II
III
IV
C
p=4.9 x 10-8
p=3.3 x 10-3
p=9.1 x 10-5
Number of paraspeckles / cell
10.0
9.0
8.0
7.0
6.0
5.0
4.0
3.0
2.0
1.0
0.0
Non-transfected (n=50)
Control (n=47)
MENε (n=63)
MENβ (n=42)

Figure S1. Quantitiative analysis of paraspeckle formation, Related to Figure 1. A, B.

Quantitative analysis of the subnuclear localization of PSF in MENε/β KO MEFs transfected with the MENβ (**A**) or MENε (**B**) expression plasmid shown in Figure 1A. PSF signals were categorized as types I–IV. The typical paraspeckle-like distribution (type II) was commonly observed in MENβ (+) cells but rarely observed in MENε (+) cells. **C**. The number of paraspeckles in cells transfected with the MENε or MENβ expression plasmid was counted. The result in Figure 1C was quantitatively analyzed. Paraspeckles were visualized by detecting both MENε/β and PSF-Flag, to distinguish paraspeckles in transfected cells from those in nontransfected cells. The average number of paraspeckles per transfected cell is plotted in the graph. The counted cell number (n) is shown below. *P*-values were calculated by Student's *t*-test. Scale bar, 10 μm.

Figure S2

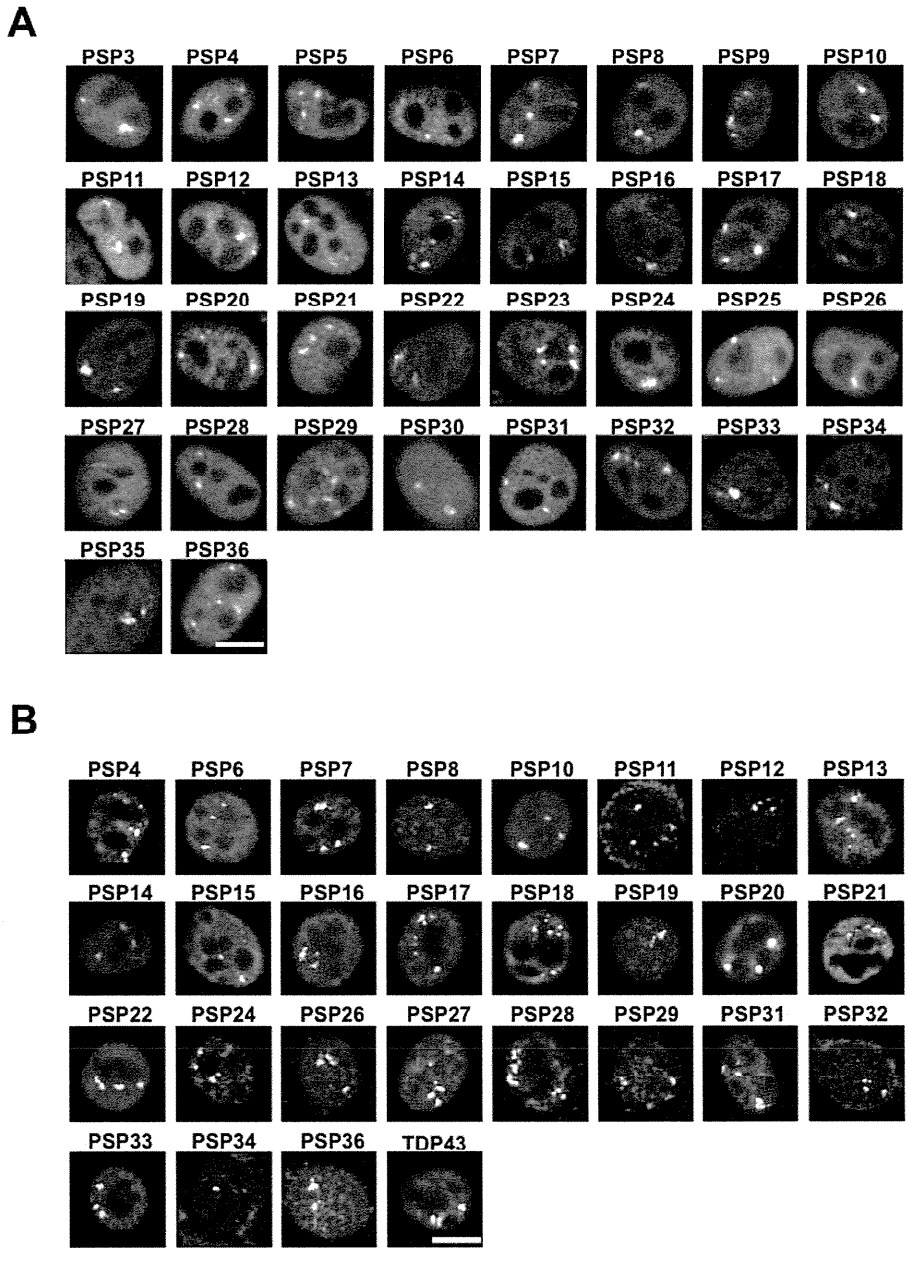
A
PSP3
PSP4
PSP5
PSP6
PSP7
PSP8
PSP9
PSP10
PSP11
PSP12
PSP13
PSP14
PSP15
PSP16
PSP17
PSP18
PSP19
PSP20
PSP21
PSP22
PSP23
PSP24
PSP25
PSP26
PSP27
PSP28
PSP29
PSP30
PSP31
PSP32
PSP33
PSP34
PSP35
PSP36
B
PSP4
PSP6
PSP7
PSP8
PSP10
PSP11
PSP12
PSP13
PSP14
PSP15
PSP16
PSP17
PSP18
PSP19
PSP20
PSP21
PSP22
PSP24
PSP26
PSP27
PSP28
PSP29
PSP31
PSP32
PSP33
PSP34
PSP36
TDP43

Figure S2. Identification of new paraspeckle protein (PSP) candidates: part I, Related to Figure 2 and Table 1. A. Confirmation of Venus signals (green) from the transfected FLJ-Venus clones that overlapped with signals of endogenous PSF (magenta). Merged images are shown. The PSP numbers refer to Table 1. **B.** Intracellular localization of endogenous proteins that were identified as new PSP candidates. The endogenous new PSPs (magenta) were detected with antibodies against the corresponding proteins. Paraspeckles were visualized with RNA-FISH of MENε/β ncRNAs (green). The localizations of seven PSPs were undetected because the corresponding antibodies were unavailable. Scale bar, 10 μm

Figure S3

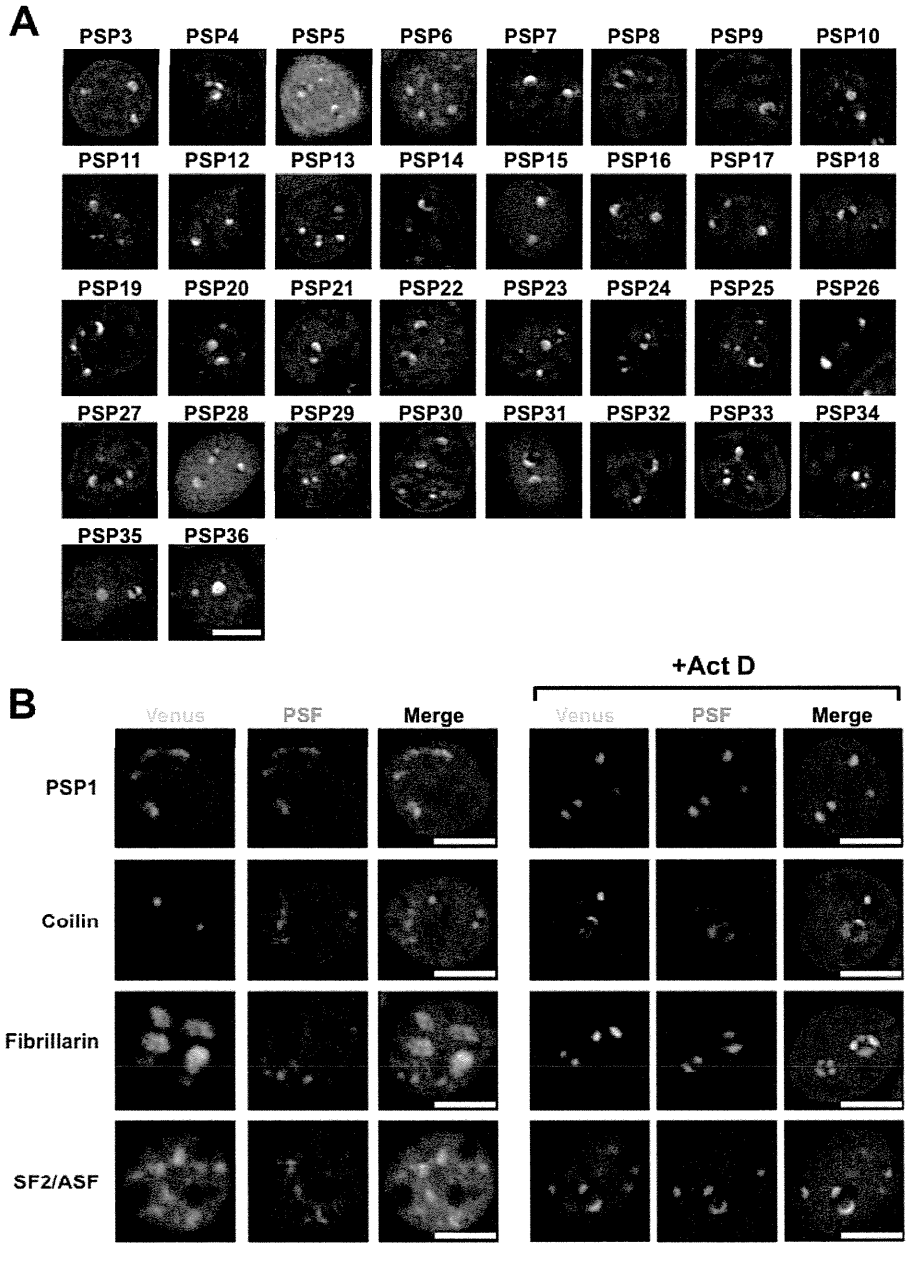
A
PSP3
PSP4
PSP5
PSP6
PSP7
PSP8
PSP9
PSP10
PSP11
PSP12
PSP13
PSP14
PSP15
PSP16
PSP17
PSP18
PSP19
PSP20
PSP21
PSP22
PSP23
PSP24
PSP25
PSP26
PSP27
PSP28
PSP29
PSP30
PSP31
PSP32
PSP33
PSP34
PSP35
PSP36
B
+Act D
Venus
PSF
Merge
Venus
PSF
Merge
PSP1
Coilin
Fibrillarin
SF2/ASF

Figure S3. Identification of new PSP candidates: part II, Related to Figure 2 and Table 1. A. Relocation of the PSP candidates to the perinucleolar caps. All of the experimental procedures were carried out as in Figure S2A, except for treatment with 0.3 μg/mL actinomycin D for 4 h. **B.** Distinct localization of nuclear body components fused with Venus. Relocation upon actinomycin D treatment is shown at the right (+Act D). Venus fusions with PSP1, coilin, fibrillarin, and SF2/ASF localize correctly to the paraspeckle, Cajal body, nucleolus, and speckle, respectively. PSF is an endogenous marker of paraspeckles. Scale bar, 10 μm.